Supporting Information

Li et al. 10.1073/pnas.1402768111

SI Text

Atomic Interaction-Based Coarse-Grained Model with a Flexible Local Potential. In this work, the calmodulin (CaM) domains are represented by a coarse-grained model in which each residue was described by one bead locating at the C_α position. The atomic interaction-based coarse-grained (AICG) model with flexible local potential developed in our previous work (termed AICG2) (1) was used with minor modifications. The energy function of modified AICG2 (termed AICG2+) was given by

$$V=\sum_I k_b\left(r^I-r_0^I\right)^2+\sum_I V_a^I\left(\theta^I\right)+\sum_I V_{dih}^I\left(\phi^I\right)+\sum_{J=I+2}\varepsilon_{1,3}^{IJ}\exp\left(-\frac{\left(r^{IJ}-r_0^{IJ}\right)^2}{2w^2}\right)+\sum_{J=I+3}\varepsilon_{1,4}^{IJ}\exp\left(-\frac{\left(\phi^I-\phi_0^I\right)^2}{2w_\phi^2}\right)+\sum_{I>J+3}^{\text{native}}\varepsilon_{\text{nloc}}^{IJ}\left[5\left(\frac{r_0^{IJ}}{r^{IJ}}\right)^{12}-6\left(\frac{r_0^{IJ}}{r^{IJ}}\right)^{10}\right]+\sum_{I>J+3}^{\text{nonnative}}\varepsilon\left(\frac{C}{r^{IJ}}\right)^{12}, \quad \text{[S1]}$$

where r^I, θ^I, and ϕ^I are virtual bond length, virtual bond angle, and dihedral angle, respectively. r^{IJ} is the distance between the Ith and Jth residues. r_0^I, ϕ_0^I, and r_0^{IJ} are the values of the corresponding variables at the reference (native) structure. $V_a^I(\theta^I)$ and $V_{dih}^I(\phi^I)$ are flexible local potentials that represent generic local propensity of given amino acids. These two terms were constructed based on a "loop-segment library" from the Protein Data Bank and are given in ref. 2. The fourth and fifth terms are the structure-based local contact potential that represents specific local interactions of the given protein structure. The coefficients $\varepsilon_{1,3}^{IJ}$, $\varepsilon_{1,4}^{IJ}$, and $\varepsilon_{\text{nloc}}^{IJ}$ can be written as $\varepsilon_{1,4}^{IJ}=\varepsilon_{1,4}W_{1,4}^{IJ}$, $\varepsilon_{1,3}^{IJ}=\varepsilon_{1,3}W_{1,3}^{IJ}$, and $\varepsilon_{\text{nloc}}^{IJ}=\varepsilon_{\text{nloc}}W_{\text{nloc}}^{IJ}$, respectively. $W_{1,3}^{IJ}$, $W_{1,4}^{IJ}$, and W_{nloc}^{IJ} are relative strengths of a given contact between the Ith and Jth residues in the corresponding terms. They were obtained based on all atom energies by energy decomposition and are specific to the studied proteins. $\varepsilon_{1,3}$, $\varepsilon_{1,4}$, and $\varepsilon_{\text{nloc}}$ are the averaged strengths of the corresponding interaction terms and were optimized by matching the fluctuations from atomistic simulations for the proteins in a dataset (3). The optimized values of $\varepsilon_{1,3}$, $\varepsilon_{1,4}$, and $\varepsilon_{\text{nloc}}$ are 1.72, 1.23, and 0.55, respectively. More details on optimizing the parameters can be found in refs. 1, 3, and 4. w and w_ϕ are the widths of the local potentials and were set as 0.15.

Integrated Modeling of Folding, Allosteric Conformational Change, and Ca^{2+} Binding. The energy landscape of allosteric proteins usually has a double-basin topology, with each basin representing a functionally relevant state. To more realistically model the conformational dynamics of CaM domains, we constructed a double-basin Hamiltonian based on the above AICG2+ potential and the multiple-basin model developed by Okazaki et al. (5), which concisely realizes conformational transitions among multiple given structures. Specifically, a double-basin potential V_{MB} was constructed by smoothly coupling two AICG2+ potentials, V_{open} and V_{closed}, and was given by

$$V_{\text{MB}}=\frac{V_{\text{open}}+V_{\text{closed}}+\Delta V}{2}-\sqrt{\left(\frac{V_{\text{open}}-V_{\text{closed}}-\Delta V}{2}\right)^2+\Delta^2}, \quad \text{[S2]}$$

where V_{open} and V_{closed} are the AICG2+ potentials with the open and closed conformations used as reference structures, respectively. There are two parameters in the multiple-basin model, energy gap ΔV and coupling term Δ. ΔV modulates the relative stability of the two functional states. In the open state of the CaM domains, a hydrophobic patch is exposed, which tends to increase the solvation energy, therefore affecting the relative stability of the two functional states. In the above AICG2+ energy function, such a solvation energy term is not explicitly included. However, the omitted effect of solvation energy can be effectively included to some extent by tuning the above parameter ΔV according to available experimental data on the populations of the open/closed states. For the C-terminal domain of CaM (CaM-C), NMR studies showed that the open conformation can have a minor but significant population (5–10%) in the absence of Ca^{2+} (6–8). In this work, ΔV was set as −3.8 kcal/mol and 1.0 kcal/mol for the N-terminal domain of CaM (CaM-N) and CaM-C, respectively, with which the calculated populations of the open conformation were around 9% at 300 K without Ca^{2+} binding for both domains. We noted that although the relative population of open conformation for the CaM-N domain was not well defined experimentally, available experimental data suggested that the open conformation is less populated in the CaM-N than that in the CaM-C in the absence of Ca^{2+} (8). Therefore, we also performed simulations with a somewhat larger ΔV, −4.2 kcal/mol, for the CaM-N, which leads to a smaller population of open conformation (~3%) without Ca^{2+} binding. We found that the major results are insensitive to the above change of ΔV value (Fig. S9). The value of Δ was set as 33.0 kcal/mol for both domains, which ensures that the transition takes place within an acceptable simulation time. Within the framework of the above double-basin energy landscape, the folding and allosteric conformational motions of CaM domains can be described in an integrated way.

In describing the Ca^{2+} binding, the implicit ligand-binding model developed in ref. 9 was used. In this model, the Ca^{2+} ions were not included explicitly (9). Instead, the energetic effect of Ca^{2+} binding was modeled by strengthening the contacting interactions formed by the liganding residues of Ca^{2+} at the open state. In this work, the two Ca^{2+} binding sites of each domain given in the Protein Data Bank (PDB) file (PDB code: 1cll) were used. The nonlocal contacts between the liganding residues of Ca^{2+} at each binding site were treated as ligand-mediated contacts, to which the following energy function was applied (9),

$$V_{\text{bind}}=\sum_{\substack{\text{ligand-mediated}\\ \text{contactpairs}}}-c_{\text{lig}}\varepsilon_0\exp\left(-\frac{\left(r^{IJ}-r_0^{IJ}\right)^2}{2\sigma^2}\right), \quad \text{[S3]}$$

where ε_0 was set as 0.55 kcal/mol. σ represents the width of interactions for the ligand-mediated contacts and was set as 0.15 Å. r_0^{IJ} is the distance between the liganding residues in the open conformation. The transitions between the Ca^{2+}-bound and unbound states were realized by Monte Carlo simulations (9). Specifically, Ca^{2+} binding is assumed to be diffusion limited and occurs with the rate $k_{\text{on}}[Ca^{2+}]$, where k_{on} is the second-order rate constant, and $[Ca^{2+}]$ is the calcium concentration. Whereas the Ca^{2+} dissociation rate is given as $k_u{}^0\exp(-\Delta V_{\text{bind}}/k_BT)$, where $k_u{}^0$ is the intrinsic off rate taken from ref. 9, ΔV_{bind} is the binding energy that depends on the conformations of the binding site, and k_BT is the thermal energy. In the simulations, $k_{\text{on}}[Ca^{2+}]$ as a whole is actively controlled by input parameters.

In Eq. **S3**, the parameter c_{lig} modulates the Ca^{2+} affinity and the relative populations of the two functional states in the Ca^{2+}-bound state. Early NMR data showed that the closed conformation is not significantly populated at high Ca^{2+} concentration (10). In this work, c_{lig} was set to 1.8 and 2.2 for the CaM-N and the CaM-C, respectively, with which the calculated populations of closed conformation are less than 3%. With the above parameters, we can calculate the populations of the two functional states as a function of binding rate $k_{on}[Ca^{2+}]$ and estimate the binding affinity. The so-determined binding affinity for the CaM-C is approximately one order of magnitude higher than that for the CaM-N, which is consistent with the available experimental data (11, 12). By mapping the calculated Ca^{2+}-binding affinity with that measured in experiment (12) for the CaM-C, we can roughly estimate the corresponding $[Ca^{2+}]$ for each input binding rate, which is shown in Fig. S9. As discussed above, the binding affinity of Ca^{2+} depends on the conformations of the binding site and therefore can be modulated by the folding and allosteric conformational motions, which are in turn controlled by the energy landscape. On the other hand, the Ca^{2+} binding itself can modify the ligand-mediated contacting interactions and therefore reshape the double-basin energy landscape. In this way, the folding, allosteric conformational change, and Ca^{2+} binding can be modeled in an integrated way.

Although the precise description of energetic consequences of the coordination events of calcium binding needs more sophisticated quantum mechanics methods and an atomically detailed structural model, the available experimentally measured binding affinity and populations of conformational states provides, although qualitatively, a reasonable parameterization of the energies at a coarse-grained level. With such a combined model, we can reasonably describe the folding, ligand binding, and allosteric motions in an integrated way.

Details of the Simulations. The coarse-gained (CG) simulations were conducted by Langevin dynamics with friction coefficient $\gamma = 0.25$. The software CafeMol2 was used for the CG simulations (13). The 3D structures of the CaM domains taken from the Protein Data Bank (PDB codes: 1cll and 1cfd) were used as reference structures in the multiple-basin model. We conducted equilibrium simulations at 300 K and 330 K with different Ca^{2+} concentrations. To mimic the single-molecule force spectroscopy experiments with pretension (11), we also conducted pretension simulations at 300 K, in which two dummy beads with certain separations were connected to the terminal residues of the CaM domains. One of the dummy beads was attached to the N-terminal residue and another dummy bead was connected to the C-terminal residue by a spring with a force constant of 0.005 $kcal{\cdot}mol^{-1}{\cdot}A^{-2}$. The force value was estimated by the distance between the C-terminal residue and the connected dummy bead. Each equilibrium simulation was conducted for around 10^9 molecular dynamics (MD) steps. We conducted multiple simulations for sufficient sampling. To characterize the folding pathways without pretension, we conducted folding simulations at 300 K, starting from unfolded structures. For each Ca^{2+} concentration, we conducted 200 independent folding simulations with the length of 5×10^7 MD steps. The initial structures were prepared by MD simulations at 1,000 K, and each of the 200 folding simulations used a different initial structure. The folding pathways with pretension were constructed based on all of the folding events collected from the equilibrium simulations. In characterizing the mechanism of allosteric transitions, we also conducted 200 independent MD simulations starting from a closed state without Ca^{2+} binding. The conformational transition events from the closed state with 0 Ca^{2+} bound (1 Ca^{2+} bound) to the open state with 1 Ca^{2+} bound (2 Ca^{2+} bound) were collected in calculating the probabilities of allosteric mechanisms due to the binding of the first (second) Ca^{2+}.

Data Analysis. In describing the folding and allosteric motions of the CaM domains, the reaction coordinates Q_{open} and Q_{closed} were used. Q_{open} and Q_{closed} represent the Q score (fraction of native contacts formed in a given snapshot) calculated with the open conformation and the closed conformation used as reference structures, respectively. For a given reference structure, the residue pairs were considered to be in native contacts if they are separated by at least four residues in sequence and the distance between the closest heavy atoms of the two residues is within 6.5 Å in the reference structure. During the CG simulations, a contact between the natively contacting residues I and J is considered to be formed if their distance is smaller than 1.2 times the C_α distance of the corresponding residue pair in the native structure. The root mean square deviation between the closed and open conformations of the CaM-N (CaM-C) is ~4.5 Å (~4.8 Å). Around 82% (77%) of the native contacts are shared by the two states of the CaM-N (CaM-C). In describing the Ca^{2+} binding, the binding energies of the two binding sites of each domain, represented by V_{bind}^{EF1} and V_{bind}^{EF2}, respectively, were used as reaction coordinates. We also used the root mean square deviations of C_α atoms ($rmsd_{open}^{EF1}$ and $rmsd_{open}^{EF2}$ for the first and second EF hands, respectively) as reaction coordinates to characterize the folding extent for each of the EF hands. In defining the conformational states, the reaction coordinate χ defined in ref. 5 was used. A negative (positive) value of the χ represents a closed (open) state. The free energy was calculated by $F(R) = -k_B T \ln(R)$, with R being the reaction coordinate.

In constructing the folding pathways in the conformational space formed by the nine substates, we need to assign the snapshots sampled in the folding simulations to each of the substates. The conformational states were assigned as follows:

Unfolded state(U): $Q_{open} < 0.5$ and $Q_{closed} < 0.5$;

Open state(O): $Q_{open} > 0.65$ or $Q_{closed} > 0.65$, and $\chi < 0.0$;

Closed state(C): $Q_{open} > 0.65$ or $Q_{closed} > 0.65$, and $\chi > 0.0$.

Similarly, the Ca^{2+}-binding states were assigned as follows:

0 Ca^{2+}-binding state: $V_{bind}^{EF1} > -0.2$ kcal/mol and $V_{bind}^{EF2} > -0.2$ kcal/mol;

1 Ca^{2+}-binding state: $V_{bind}^{EF1} \le -1.0$ kcal/mol and $V_{bind}^{EF2} > -0.2$ kcal/mol or

$V_{bind}^{EF2} \le -1.0$ kcal/mol and $V_{bind}^{EF1} > -0.2$ kcal/mol;

2 Ca^{2+}-binding state: $V_{bind}^{EF1} \le -1.0$ kcal/mol and $V_{bind}^{EF2} \le -1.0$ kcal/mol.

Based on the above criteria for defining conformational states and Ca^{2+}-binding states, we can roughly assign the snapshots to each of the nine substates and therefore construct the folding pathways. The folding/unfolding trajectories may involve the back-and-forth transitions, which lead to loops in the folding routes. These loops are removed from the folding routes. In the above state assignment, a number of cutoff values were used. Changing these cutoff values can affect the quantitative results (e.g., the probability of a certain folding pathway), but the major findings are not changed. We emphasize that there are more than nine possible states if we also consider the partially folded conformations in which only one of the two EF hands is well folded. However, due to the high cooperativity of the CaM domains as observed in this work (Fig. S2) and in previous experiments (11, 14, 15), the nine-state representation can well capture the major features of the conformational fluctuations and Ca^{2+} binding. With the nine-state representation, some partially folded structures may be assigned as unfolded states.

1. Li W, Terakawa T, Wang W, Takada S (2012) Energy landscape and multiroute folding of topologically complex proteins adenylate kinase and 2ouf-knot. *Proc Natl Acad Sci USA* 109(44):17789–17794.
2. Terakawa T, Takada S (2011) Multiscale ensemble modeling of intrinsically disordered proteins: p53 N-terminal domain. *Biophys J* 101(6):1450–1458.
3. Li W, Wolynes PG, Takada S (2011) Frustration, specific sequence dependence, and nonlinearity in large-amplitude fluctuations of allosteric proteins. *Proc Natl Acad Sci USA* 108(9):3504–3509.
4. Li W, Yoshii H, Hori N, Kameda T, Takada S (2010) Multiscale methods for protein folding simulations. *Methods* 52(1):106–114.
5. Okazaki K, Koga N, Takada S, Onuchic JN, Wolynes PG (2006) Multiple-basin energy landscapes for large-amplitude conformational motions of proteins: Structure-based molecular dynamics simulations. *Proc Natl Acad Sci USA* 103(32):11844–11849.
6. Malmendal A, Evenäs J, Forsén S, Akke M (1999) Structural dynamics in the C-terminal domain of calmodulin at low calcium levels. *J Mol Biol* 293(4):883–899.
7. Chen YG, Hummer G (2007) Slow conformational dynamics and unfolding of the calmodulin C-terminal domain. *J Am Chem Soc* 129(9):2414–2415.
8. Kuboniwa H, et al. (1995) Solution structure of calcium-free calmodulin. *Nat Struct Biol* 2(9):768–776.
9. Okazaki K, Takada S (2008) Dynamic energy landscape view of coupled binding and protein conformational change: Induced-fit versus population-shift mechanisms. *Proc Natl Acad Sci USA* 105(32):11182–11187.
10. Chou JJ, Li S, Klee CB, Bax A (2001) Solution structure of Ca(2+)-calmodulin reveals flexible hand-like properties of its domains. *Nat Struct Biol* 8(11):990–997.
11. Stigler J, Rief M (2012) Calcium-dependent folding of single calmodulin molecules. *Proc Natl Acad Sci USA* 109(44):17814–17819.
12. Bayley PM, Findlay WA, Martin SR (1996) Target recognition by calmodulin: Dissecting the kinetics and affinity of interaction using short peptide sequences. *Protein Sci* 5(7): 1215–1228.
13. Kenzaki H, et al. (2011) CafeMol: A coarse-grained biomolecular simulator for simulating proteins at work. *J Chem Theory Comput* 7(6):1979–1989.
14. Junker JP, Ziegler F, Rief M (2009) Ligand-dependent equilibrium fluctuations of single calmodulin molecules. *Science* 323(5914):633–637.
15. Gifford JL, Walsh MP, Vogel HJ (2007) Structures and metal-ion-binding properties of the Ca2+-binding helix-loop-helix EF-hand motifs. *Biochem J* 405(2):199–221.

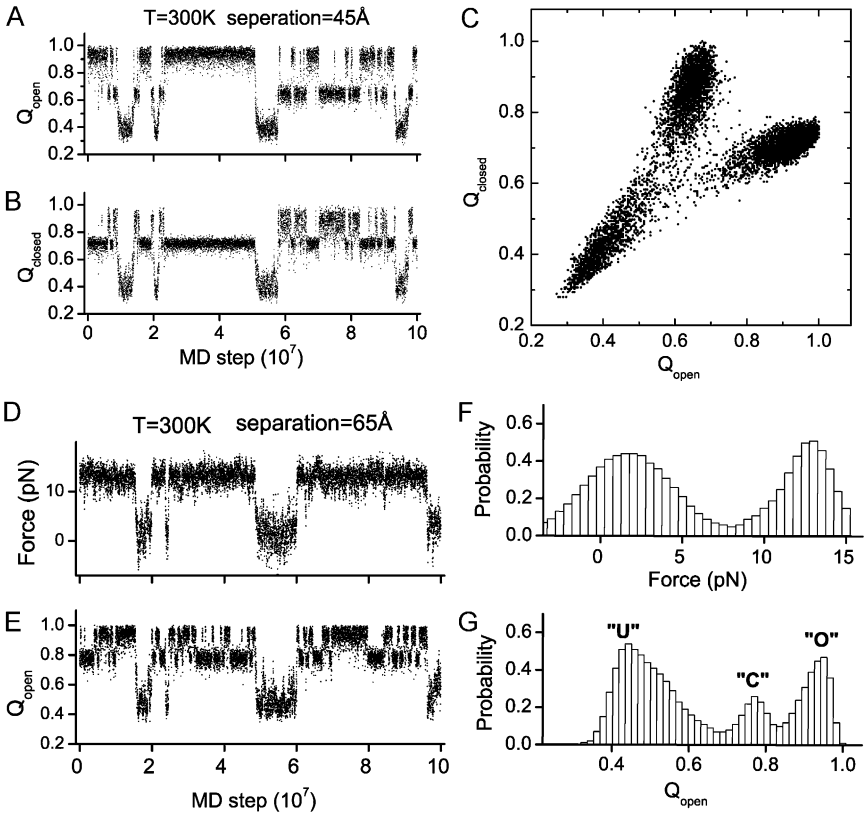

Fig. S1. (*A* and *B*) Representative trajectory for the isolated CaM-C monitored by Q_{open} (*A*) and Q_{closed} (*B*) for the pretension simulations at 300 K with Ca^{2+} concentrations of 1.7 μM. (*C*) Correlation plot of the same trajectory projected on Q_{open} and Q_{closed}. (*D* and *E*) Representative trajectory for the isolated CaM-N monitored by force (*D*) and Q_{open} (*E*) for the pretension simulations at 300 K with Ca^{2+} concentrations of 3.3 μM. (*F* and *G*) Distributions of force value (*F*) and Q_{open} (*G*) for the pretension simulations of the isolated CaM-N.

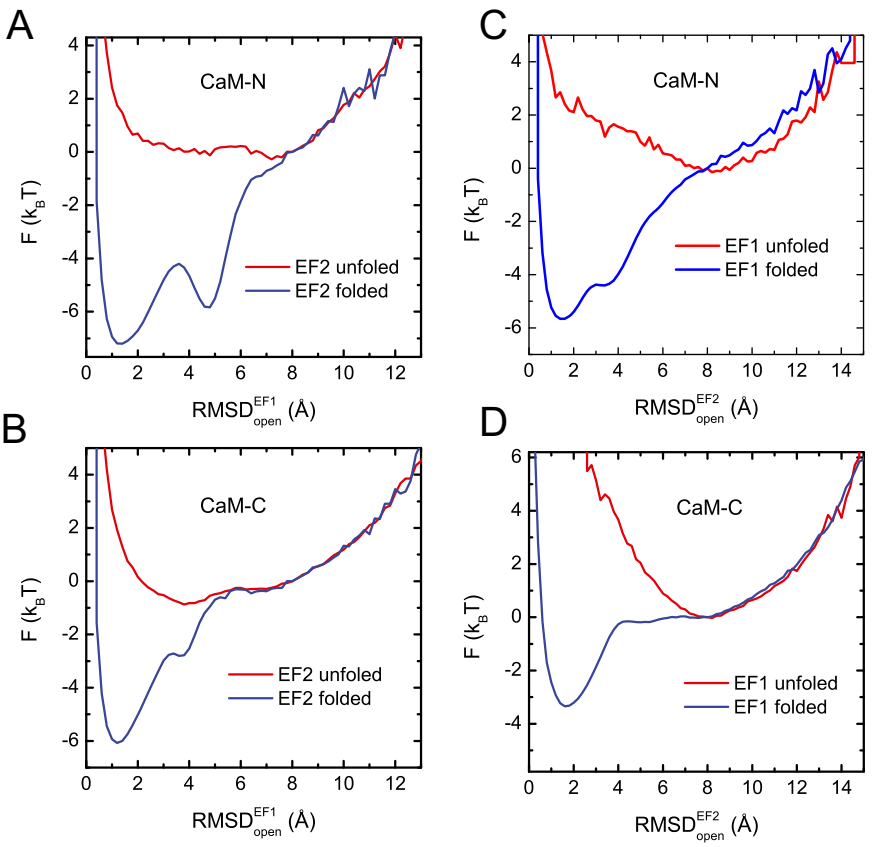

Fig. S2. (*A–D*) Folding cooperativity between the two EF hands of the isolated domains of CaM (*A* and *C*, CaM-N; *B* and *D*, CaM-C). (*A* and *B*) Free energy profile projected on the reaction coordinate $\text{rmsd}^{\text{EF1}}_{\text{open}}$ ($\text{rmsd}^{\text{EF2}}_{\text{open}}$) when the EF-hand 2 (EF-hand 1) is folded (blue) or unfolded (red) for the isolated CaM-N at 330 K with the Ca^{2+} concentration of 330.0 μM. (*C* and *D*) Same as *A* and *B* but for the isolated CaM-C. One can see that the folding of one EF hand can significantly increase the stability of another EF hand, suggesting high folding cooperativity between the two EF hands.

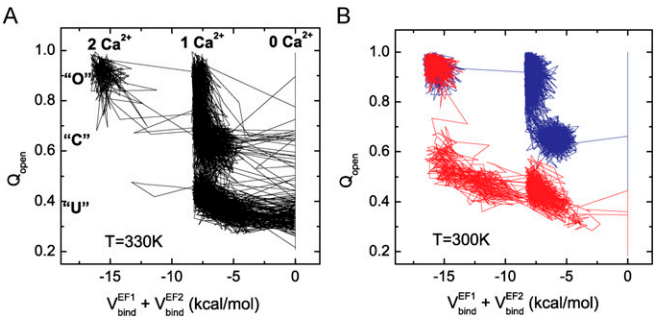

Fig. S3. (*A*) Representative trajectory by MD simulations at 330 K with Ca^{2+} concentration of 3.3 μM for the isolated CaM-C projected on the reaction coordinates Q_{open} and total binding energy of the two binding sites. (*B*) Representative folding trajectories with "combined spontaneous folding and induced-fit" mechanism (blue) and "binding-induced folding" mechanism (red) by MD simulations at 300 K for the isolated CaM-C projected on the same reaction coordinates with Ca^{2+} concentrations of 3.3 μM and 330.0 μM, respectively. In the blue trajectory, the back-and-forth transition loop "C" → "O" → "C" with the 0 Ca^{2+}-bound state, which cannot be clearly identified in the plot, was not included in the folding pathway.

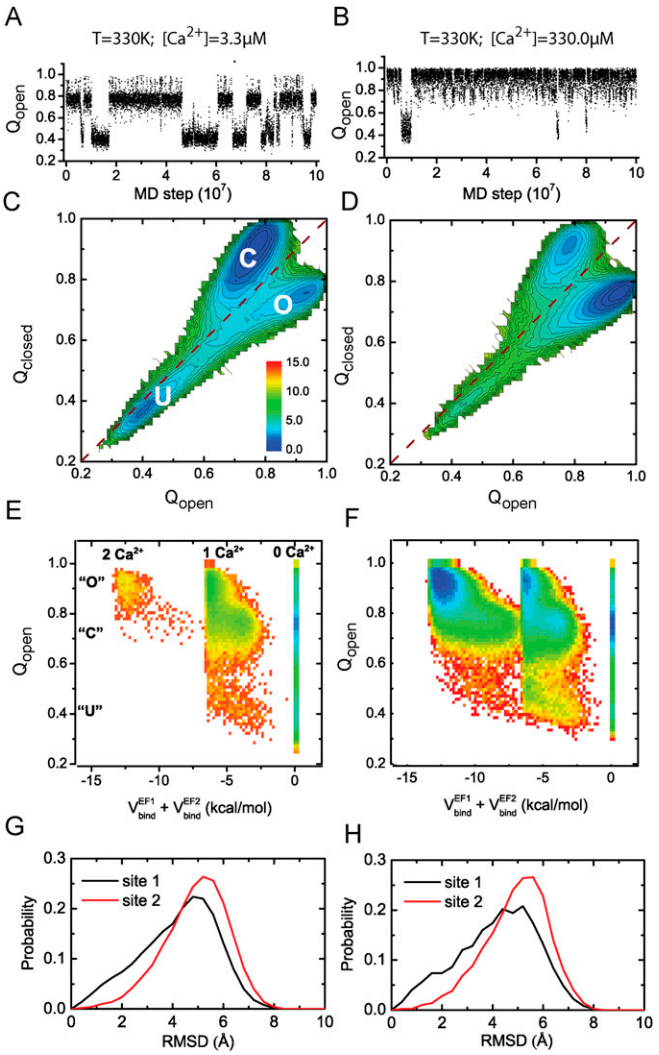

Fig. S4. (*A* and *B*) Representative trajectories for the isolated CaM-N monitored by Q_{open} for the simulations at 330 K with Ca^{2+} concentrations of 3.3 μM (*A*) and 330.0 μM (*B*). (*C* and *D*) Free energy profiles of the isolated CaM-N on the reaction coordinates Q_{open} and Q_{closed} at 330 K with Ca^{2+} concentrations of 3.3 μM (*C*) and 330.0 μM (*D*). The dashed lines correspond to the diagonal line of the 2D free energy surfaces. (*E* and *F*) Free energy profiles projected on the reaction coordinates Q_{open} and total binding energy of the two binding sites with Ca^{2+} concentration of 3.3 μM (*E*) and 330.0 μM (*F*) at 330 K for the CaM-N. The unit of the free energy is k_BT. (*G* and *H*) Distributions of the rmsd (to the native structures of the binding sites) of the two Ca^{2+}-binding sites at the unfolded state without Ca^{2+} binding with Ca^{2+} concentration of 3.3 μM (*G*) and 330.0 μM (*H*) at 330 K for the isolated CaM-N. The liganding residues of each binding site locate at a 12-residue loop region and therefore have short separations in sequence. One can see that even in the unfolded state, the residues in the binding sites can form near native conformations (e.g., with rmsd < 2.0 Å) with minor but significant probability before the Ca^{2+} binding, which makes the Ca^{2+} binding possible even at the unfolded state as observed here and in Fig. 4 of the main text.

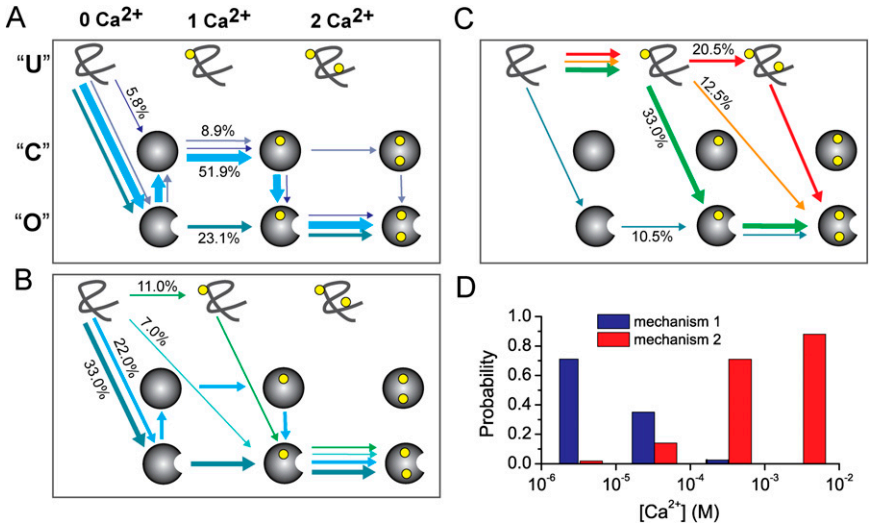

Fig. S5. (*A*–*C*) Folding pathways of the isolated CaM-N with the Ca^{2+} concentrations of 3.3 μM (*A*), 33.0 μM (*B*), and 330.0 μM (*C*) at 300 K. The closed state is represented by a solid sphere and the open state by a sphere with a notch. The yellow spheres represent Ca^{2+} ions. The end point of the folding pathway was set as an open state with two Ca^{2+} ions bound. The probabilities of the pathways are represented by line breadth and percentage number, and different pathways are represented by arrow lines with different colors. In calculating the probability of the folding pathways, 200 independent folding simulations were conducted starting from fully unfolded initial structures. Only the four most populated pathways are shown. (*D*) Probability of the folding mechanisms, combined spontaneous folding and induced fit (mechanism 1, blue) and binding-induced folding (mechanism 2, red), at three Ca^{2+} concentrations. Note that the probability not only includes the pathway with blue (red) color shown, but also includes all other pathways satisfying the mechanism 1 (mechanism 2). We have also observed other folding mechanisms. For example, the protein may first fold spontaneously to the open (or closed) state and then bind Ca^{2+} ions directly (or bind Ca^{2+} ions after converting to the open state), which can be termed a "conformational selection" mechanism. Particularly, for the CaM-N, the probability of the conformational selection mechanism becomes significant (~39%) at intermediate Ca^{2+} concentration (33.0 μM). We note that transition from one Ca^{2+}-bound closed state to two Ca^{2+}-bound closed states is rare for both CaM-N (this figure) and CaM-C (Fig. 4 of main text), which results from the high cooperativity between the two EF hands. Due to the cooperativity, the binding of one Ca^{2+} can induce the conformational change of the whole CaM domain from a closed state to an open state with a high probability, which reduces the transition from one Ca^{2+}-bound closed state to two Ca^{2+}-bound closed states.

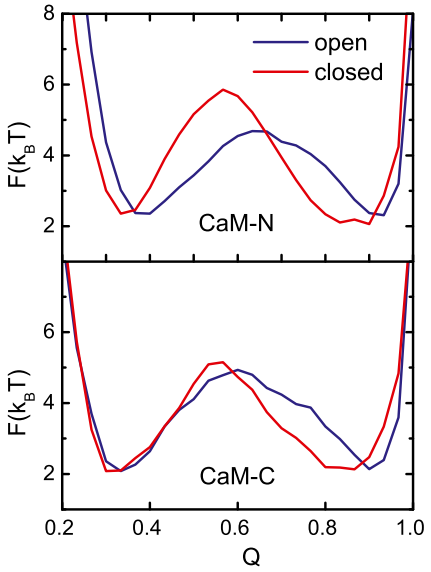

Fig. S6. One-dimensional free energy landscape on the reaction coordinate *Q*, the fraction of folded native contacts, based on the folding simulations by the single-basin Hamiltonian with the structures at closed (red) and open (blue) states used as the reference structures at the folding temperature for the isolated CaM-N (*Upper*) and CaM-C (*Lower*).

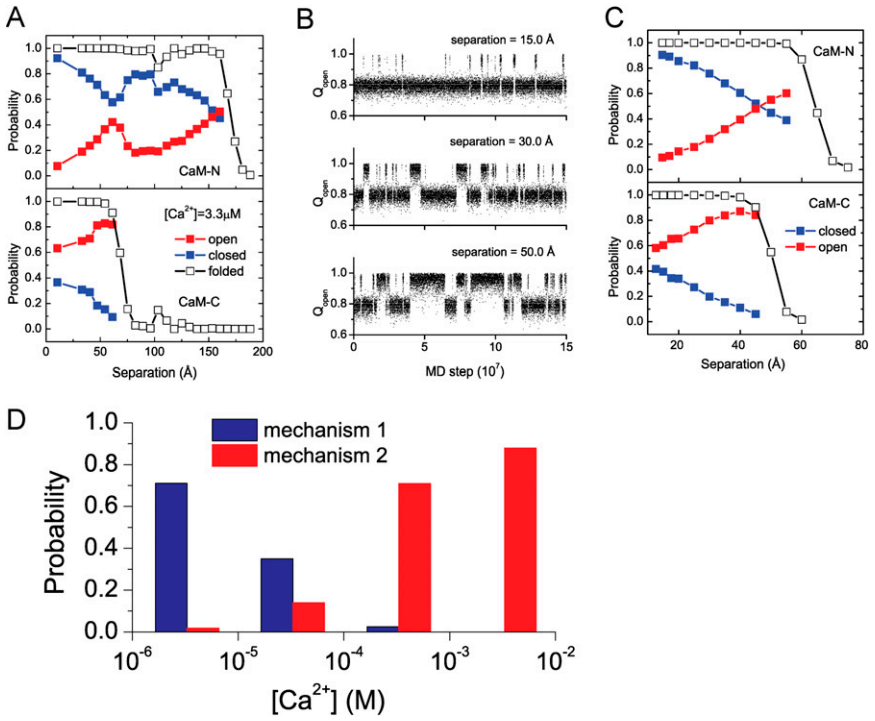

Fig. S7. (*A*) Populations of the closed (blue), open (red), and folded (black) states of the CaM-N (*Upper*) and CaM-C (*Lower*) of the full-length CaM as a function of separations between the two dummy beads connected to the terminal residues at 300 K and $[Ca^{2+}] = 3.3$ μM. We can see that with the separation of the dummy beads increasing, the population of the open (closed) state increases (deceases) for both domains, which suggests that the pretension can modulate the relative populations of the functional states. A possible reason of the pretension-induced population shift is that the terminal residues of the open state have larger separation than that of the closed state. Consequently, pretension favors the open state. We also observed that once the CaM-C gets unfolded, the population of the open (closed) state of the CaM-N drops (increases) to some extent, which is due to the release of tension between the terminal residues by CaM-C unfolding. Such results suggest that the pretension of the full-length CaM can introduce certain correlation between two domains. (*B*) Representative trajectories of isolated CaM-N at three different pretensions. (*C*) Populations of the closed (blue), open (red), and folded (black) states of the isolated CaM-N (*Upper*) and CaM-C (*Lower*) as a function of separations between the two dummy beads connected to the terminal residues of each domain at 300 K and Ca^{2+} concentration of 3.3 μM. Similar to the results of full-length CaM, with the separation of the dummy beads increasing, the population of the open (closed) state increases (deceases) for both domains. (*D*) Probability of the folding mechanisms, combined spontaneous folding and induced fit (mechanism 1, blue) and binding-induced folding (mechanism 2, red), at four separations with Ca^{2+} concentration of 3.3 μM for the isolated CaM-C. One can see that increasing the tension tends to favor the binding-induced folding mechanism, demonstrating the modulation of the folding mechanism by applying tension.

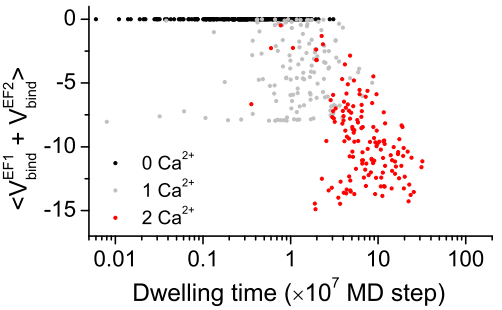

Fig. S8. Correlation plot between the averaged binding energies and dwelling time of the folded conformations for the pretension simulations of the isolated CaM-C at 300 K with Ca^{2+} concentration of 1.7 μM. <...> represents the average over the dwelling time of a folded state.

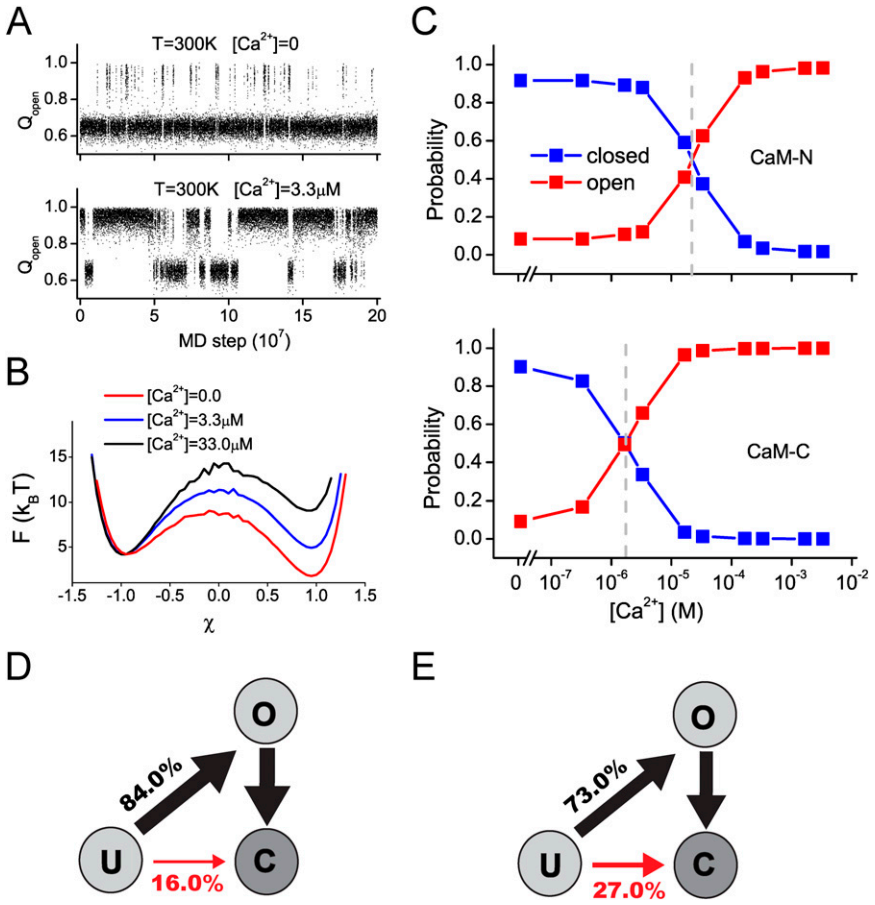

Fig. S9. (*A*) Representative trajectory for the isolated CaM-C monitored by Q_{open} with Ca^{2+} concentration of 0 (*Upper*) and 3.3 μM (*Lower*). (*B*) Free energy profile projected on the reaction coordinate χ at three different concentrations of Ca^{2+} ions ($\chi < 0$, open state; $\chi > 0$, closed state). (*C*) Populations of the closed (blue) and open (red) states of the isolated CaM-N (*Upper*) and CaM-C (*Lower*) as a function of Ca^{2+} concentration at 300 K. As expected, without Ca^{2+} binding, the populations of the open state are less than 10%. At high Ca^{2+} concentrations, the populations of the closed state are less than 3.0%. The obtained relative populations of the two functional states are within the range of available experimental restraint. In addition, with the increasing of the Ca^{2+} concentration, the population of the open state increases and then saturates at high concentrations. Compared with the CaM-N, the transition concentration of the CaM-C is much lower than that of the CaM-N as shown by the left shift of the dashed line, suggesting the higher Ca^{2+} affinity of the CaM-C compared with that of the CaM-N, which is consistent with experimental observations. (*D* and *E*) Folding pathways on the conformational space formed by three states, i.e., unfolded state (U), closed state (C), and open state (O) with the Ca^{2+} concentration of 0 for the isolated CaM-N domain with $\Delta V = -3.8$ kcal/mol (*D*) and −4.2 kcal/mol (*E*). The probabilities of the pathways are represented by line breadth and percentage number, and different pathways are represented by arrow lines with different colors. With these two values of the parameter ΔV, the populations of the open conformation with no calcium are around 9% and 3%, respectively. One can see that although the open conformation with $\Delta V = -4.2$ kcal/mol is much less stable, the U → O → Cpathway still dominates.